Novel elastic, lattice dynamics and thermodynamic properties of metallic single-layer transition metal phosphides: 2H-M_2P (Mo_2P, W_2P, Nb_2P and Ta_2P)

Jiuren Yin[1,2*], Bozhao Wu[2], Yanggang Wang[3], Zhimi Li[2], Yuanpeng Yao[2], Yong Jiang[1,2], Yanhuai Ding[1,2*], Fu Xu[2], Ping Zhang[1,2]

1. Institute of Rheological Mechanics, Xiangtan University, Hunan 411105, China

2. College of Civil Engineering and Mechanics, Xiangtan University, Hunan 411105, China.

3. Fritz-Haber-Institut der Max-Planck-Gesellschaft, Berlin-Dahlem, 14195 Germany

Email: yinjr@xtu.edu.cn (J.R.Yin) and yhding@xtu.edu.cn (Y.H. Ding).

Abstract Recently a surge of interest has been poured into research of two dimensional (2D) phosphides due to their unique physical properties and wide applications. Transition metal phosphides 2H-M_2Ps (Mo_2P, W_2P, Nb_2P and Ta_2P) show considerable catalytic activity and energy storage potential. However, the electronic structure and mechanical properties of 2D 2H-M_2Ps are still unrevealed. Here first-principles calculations are employed to investigated the lattice dynamics, elasticity and thermodynamics properties of 2H-M_2Ps. Results show that M_2Ps with lower stiffness exhibit remarkable lateral deformation under unidirectional loads. Due to the largest average Grüneisen parameter, single-layer Nb_2P has the strongest anharmonic vibrations, resulting in the highest thermal expansion coefficient. The lattice thermal conductivity of Ta_2P, W_2P and Nb_2P is contradictory to the classical theory which would expect a smaller thermal conductivity due to the much heavier atom mass. Moreover, the calculations also demonstrate that the thermal conductivity of Ta_2P is the highest, as well as the lowest thermal expansion, owing to its weak anharmonic phonon scattering and the lowest average Grüneisen parameter. The insight provided by this study can be useful for future experimental and theoretical studies concerning 2D transition metal phosphides materials.

Keywords: transition metal phosphides, elastic properties, lattice dynamics, thermodynamic properties

1. Introduction

Since the discovery of graphene in 2004[1], its outstanding properties such as strong mechanical strength[2], excellent carrier mobility[3] and superior thermal conductivity[4] have been disclosed. However, some applications of graphene were restricted due to its intrinsic zero band-gap and relatively simple chemistry in energy storage devices and high-performance field-effect transistors (FET)[5, 6]. Nonetheless, the field of two dimensional (2D) materials has undergone rapid development. Exploration of new 2D materials including mono-elemental materials and abundant elemental composition are of great interest, such as 2D black phosphorus-like arsenic[7], tellurene[8], honeycombed silicon-carbon[9-11], layered chalcogenides[12] and transition metal dichalcogenides (TMDs)[13, 14]. Meanwhile, a collection of 2D transition metal carbides and nitrides, labeled as MXenes have been exploited[15-19]. Present research reveals that MXenes exhibit advantageous thermal conductivity and hydrophilic surfaces, high elastic moduli, carrier mobility and specific surface areas[20-23]. Particularly, low metal diffusion barriers on their surfaces recommend MXenes for application in energy storage and functional polymer composites[19, 24, 25]. Generally, MXenes can be fabricated by the selective chemical etching of MAX Phases. MAX phases are denoted by a general formula of $M_{n+1}AX_n$ (n=1~3), where 'M' represents early transition metals, 'A' is a main group element (mostly groups 13 and 14), and 'X' represents carbon and/or nitrogen[15].

The family of 2D MXenes has gone through bountiful expansion in recent years. One recent contender that has received significant attention is transition metal carbides (TMCs) with many intriguing properties and applications since their 2D crystals have been grown by chemical vapor deposition (CVD)[26, 27]. More recently, one-step direct synthesis of large-area 2D Mo_2C-on-graphene film by molten copper-catalyzed chemical vapor deposition (CVD) was reported[28]. *Ab* initio results announce that Li-adsorbed Mo_2C

monolayer possesses a high theoretical capacity of 526 $mAh \cdot g^{-1}$ and a low average electrode potential of 0.14 eV[25], demonstrating the tempting application of Mo_2C monolayer as an appealing anode material for Li-ion batteries. By using theoretical calculations, monolayer Mo_2C presents a superconductor characteristic with tunable critical temperature (0~13 K) by the surface termination (-O, -H and -OH)[29].

Recently, two dimensional (2D) transition metal phosphides (2H-Mo_2P) have been reported as an anode material for Li- and Na-ions with superionic conductivity[30]. Based on the first-principles calculations, we propose three 2D transition metal phosphides, labeled as 2H-W_2P, 2H-Nb_2P and 2H-Ta_2P, respectively. The calculated phonon dispersions spectra demonstrate their highly dynamical stability. To reveal the fundamental properties of the transition metal phosphides labeled as 2H-M_2P (M= Mo, W, Nb, Ta), lattice dynamics and thermodynamic properties, electronic and elastic properties were characterized by using theoretical calculations, aiming to facilitate the synthesis and further applications of transition metal phosphides.

2. Computational Details

Based on the density functional theory (DFT), first-principles calculations are implemented in the Vienna *ab* initio simulation package (VASP)[31-33]. The projector augmented wave (PAW) pseudopotential is modeled to treat the interactions between electrons and irons[34]. General gradient approximation (GGA) is used with the Perdew–Burke–Ernzerhof (PBE) functional to describe the exchange and correlation interactions between electrons[35]. The energy cutoff is set to 500 eV for all calculations. The Monkhorst−Pack k-point sampling is used for the Brillouin zone integration: 19 × 19 × 1 for relaxation, and 45 × 45 × 1 for self-consistent calculations[30, 36]. The cell parameters and ionic positions are fully optimized until the residual force on each atom is less than 0.01 eV/Å. A vacuum space of 20 Å is used to avoid the interaction between periodic images. The electronic properties are calculated by using GGA-PBE functional.

Moreover, the electronic band structures are further confirmed by calculations with hybrid functional method (HSE06)[37].

Phonon dispersions spectra and projected densities of states (PDOS) were obtained by combining density-functional perturbation theory (DFPT)[38] with the open source code Phonopy[39]. Thermal properties were calculated with harmonic approximation, then constant volume heat capacity C_V, Helmholtz free energy F, and entropy S can be computed as functions of temperature. Heat capacity at constant pressure (C_P) and temperature-dependent thermal properties can be obtained with quasi-harmonic approximation (QHA). Besides, lattice thermal conductivities were investigated by solving linearized Boltzmann transport equation within the single-mode relaxation time approximation (RTA), as implemented in the open code Phono3py[40]. The interatomic force constants (IFCs) were calculated by the finite displacement method. The second- and third-order harmonic IFCs were obtained by using finite displacement method with finite atomic displacements of 0.03 Å. To compute lattice thermal conductivities, the reciprocal spaces of the primitive cells were sampled using the 45×45×1 meshes.

3. Results and discussions

3.1 Lattice structures and dynamical stability

As shown in **Figure. 1a**, all the 2D 2H-M_2P structures have the hexagonal lattice symmetry of space group D^1_{3h} ($P\bar{6}m2$), with two M and one P atom in a primitive unit cell. 2H-M_2P is consisted of monolayers that are vertically stacked in M−P−M sequence as 2H-Mo_2C[29], with two M atomic layers sandwiching a single P layer in a mirror-symmetric manner (**Figure 1b and 1d**). The fully relaxed structures have an equilibrium lattice constant of 3.065, 3.031, 3.153 and 3.116 Å for 2H-Mo_2P, -W_2P, -Nb_2P and -Ta_2P, respectively. The lattice parameters, bond length, and cohesive energies are listed in **Table 1**. The lattice parameter and bond

length of Mo_2P well coincide with the reported (a=3.064 Å, $bond_{Mo\text{-}P}$= 2.347 Å)[30]. Structural stability can be inferred from the cohesive energy per atom which is defined as $E_{coh} = (2E_M + E_P - E_{M_2P})/3$, where E_M, E_P and E_{M2P} denote the energy of isolated M atom, P atom and total energy of the primitive unit cell, respectively. The calculated cohesive energies per atom of 2H-Mo_2P, -W_2P, -Nb_2P and -Ta_2P are 6.995, 6.095, 5.524 and 6.136 eV/atom. The equilibrium distances of M−P bonds are 3.347, 3.366, 3.456 and 3.453 Å, respectively. Here the 2D 2H-M_2P structures are more stable than 2H-MoS_2 (with a E_{coh}=4.979 eV/atom), indicating monolayer Mo_2P is most stable architecture among the four 2D crystals, corresponding to its shortest bond length of Mo-P. Like 2H-Mo_2C[29], the 2H-M_2P may also have 1T phase as illustrated in **Table S1**. The optimized total energy of 1T phases is little larger than that of 2H phases. **Table S1** shows the optimized lattice parameters and cohesive energies of 1T-M_2P. Compared to 2H-M_2P, the cohesive energy of 1T-M_2P is smaller than that of 2H-M_2P, indicating that 2H-M_2P is more stable.

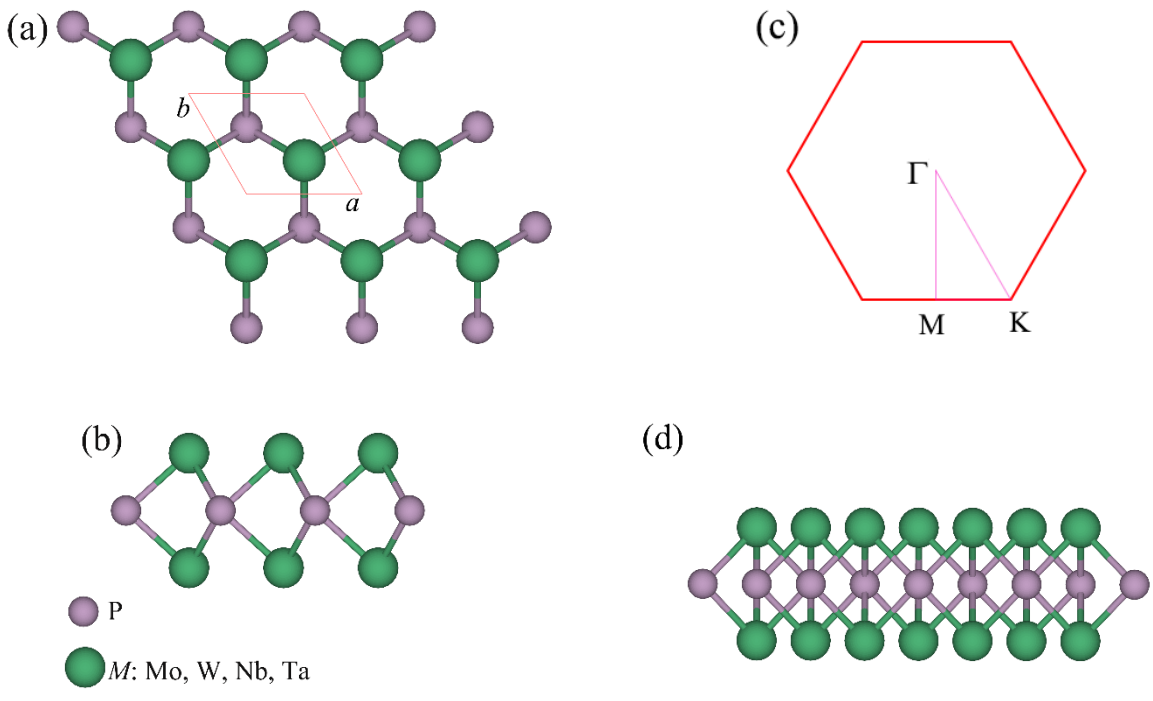

Figure 1 (a) Top, (b) and (d) side views of the single-layer transition metal phosphides, labeled as 2H-M_2P. In (a) the red region indicates the primitive unit cell, a=b are the lattice constants (a=b). (c) First Brillouin

zone with high-symmetry points labeled.

Table 1 Lattice parameters *a* and *b*, the bond length of *M*-P bond$_{M\text{-P}}$, the thickness of *M*-P-*M* $d_{M\text{-}M}$ and cohesive energies E_{coh} of 2D monolayer 2H-M_2P in unitcell (*M*= Mo, W, Nb, Ta).

	a (Å)	*b* (Å)	bond$_{M\text{-P}}$ (Å)	$d_{M\text{-}M}$ (Å)	E_{coh} (eV/atom)
Mo_2P	3.065	/	2.347	3.084	6.995
W_2P	3.031	/	2.366	3.186	6.095
Nb_2P	3.153	/	2.456	3.296	5.524
Ta_2P	3.116	/	2.453	3.336	6.136

The electron localization function (ELF) of these four configurations is also characterized as depicted in **Figure 2**. The ELFs indicate the degree of electron localization which is helpful for the analysis of bonding characters[41]. It's clear that a covalent bond *M*-*P* is formed. The ELF value is 0.79847, 0.80354, 0.83242 and 0.83463 for Mo_2P, W_2P, Nb_2P and Ta_2P, respectively. The difference of ELF value between the up-down two *M* metal atoms is about 0.3~0.4, indicating the electron delocalization. One anticipated finding is that the electron localization around W atoms is higher than that around the other three atoms (Mo, Nb, and Ta). Dynamical stability of the M_2P structures is investigated by calculating phonon dispersion spectra (along Γ-M-K-Γ path over Brillouin zone) and projected densities of states (PDOS) of every atomic donors in three directions. As illustrated in **Figure 3**, the absence of imaginary frequencies in the phonon spectra throughout the Brillouin zone demonstrates the highly dynamical stability of all M_2P structures. From the calculated PDOS, apparently, high optical phonons vibrations should be mainly attributed to the donors of P atoms in *y*- and *z*-directions, while the low optical and acoustic phonons vibrations are governed by the larger atomic

mass M in y- and z-directions. As a result being known from phonon frequencies over the Brillouin zone, thermal properties are calculated as illustrated in **Figure S2**. The calculated results establish the notable energetic and dynamical stability of 2H-M_2P, and will facilitate and motivate the further synthesis of transition metal phosphides.

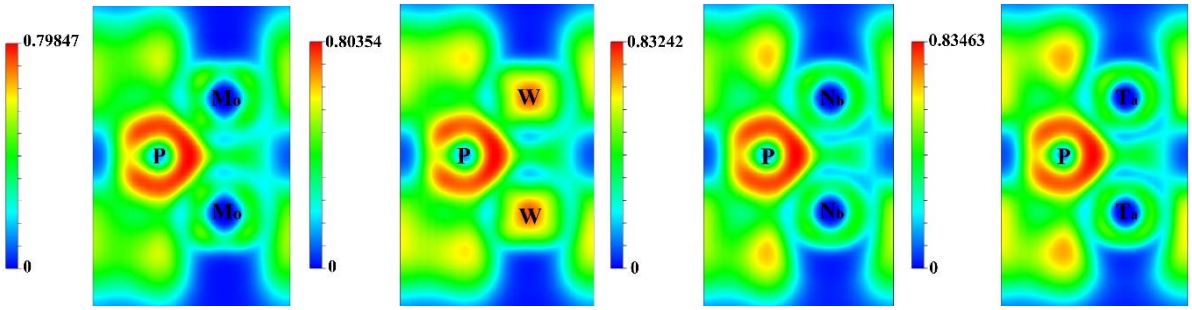

Figure 2 Electron localization function (ELF) of the single-layer M_2P, diagrams in turn from left-to-right: Mo_2P, W_2P, Nb_2P and Ta_2P.

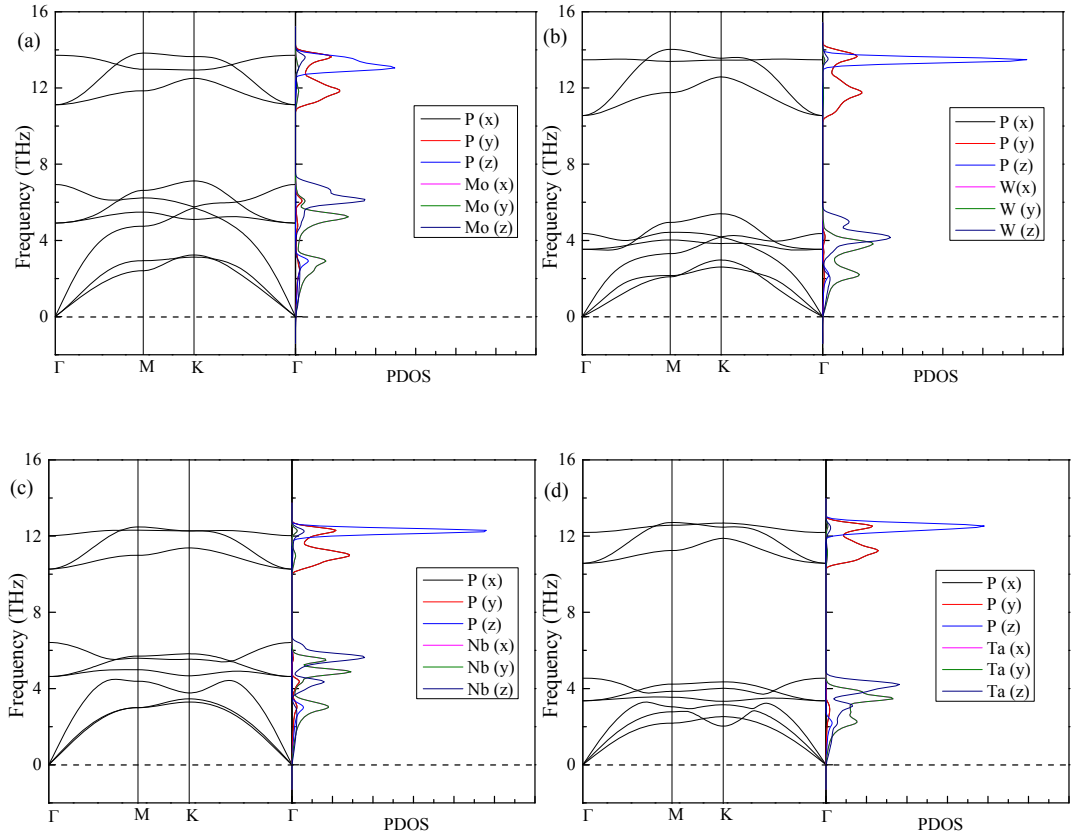

Figure 3 Phonon dispersion spectra (left) and projected density of state (right) of monolayer M_2P implemented within a 3×3×1 super cell, by using GGA-PBE functional to describe the exchange-correlation potential.

3.2 Elastic and electronic properties

The elastic properties of monolayer M_2P can be characterized according to the method mentioned by Andrew[42] without considering the film thickness. The 2D elastic constants of hexagonal lattices are defined as c_{11}, c_{22}, c_{12}, and c_{66}. Due to the symmetry, the hexagonal structures have the two relations that $c_{11} = c_{22}$ and $c_{66} = 1/2(c_{11} - c_{12})$. Before that, weak interactions (primarily van der Waals interactions) between two M_2P surfaces are firstly confirmed by optimizing the configurations of a stacked assembly of two layer with using vdW correction methods (DFT-D3)[43], which determines the equilibrium interlayer distance d_{vdW}. The effective single-layer thickness t is $d_{vdW} + d_{M\text{-}M}$. The elastic constant matrix of these single-layer M_2P is calculated as shown in **Table 2**. The elastic properties of the hexagonal lattice of M_2P can be obtained. The layer modulus and shear modulus are expressed as

$$\gamma = \frac{1}{4}(c_{11} + c_{22} + 2c_{12}) \quad \text{and} \quad G^{2D} = c_{66} \tag{1}$$

2D in-plane stiffness (Young's moduli) for strains and Poisson's ratio in the Cartesian [10] and [01] directions can be expressed as:

$$S_{[10]} = \frac{c_{11}c_{22} - c^2_{12}}{c_{22}} \quad \text{and} \quad S_{[01]} = \frac{c_{11}c_{22} - c^2_{12}}{c_{11}} \tag{2}$$

$$\nu^{2D}_{[10]} = \frac{c_{12}}{c_{22}} \quad \text{and} \quad \nu^{2D}_{[01]} = \frac{c_{12}}{c_{11}} \tag{3}$$

In-plane stiffness in the Cartesian [10] and [01] directions, respectively, are equal in value due to the hexagonal lattice, as well as Poisson's ratio. As shown in **Table 2**, calculated stiffness of monolayer Mo_2P is 53.6 N/m (GPa·nm) which is well consistent with the reported (56 GPa·nm)[30]. Compared with the stiffness of MoS_2 (~140 N/m), the investigated stiffness of M_2Ps is smaller than half that of MoS_2, indicating M_2P architectures are softer materials which would facilitate the application of external strain. Magically, monolayer M_2Ps exhibit an excellently lateral deformation capacity in consideration of themselves larger Poisson's ratio (> 0.5) when applied unidirectional strain. Among the 2D M_2Ps, single-layer Ta_2P has the highest stiffness, 63 N/m (63 GPa·nm), corresponding to the Poisson's ratio of 0.538. Most surprisingly, single-layer Nb_2P has the lowest stiffness of 4.3 N/m (4.3GPa·nm) and best lateral deformation (Poisson's ratio of 0.961), which demonstrate single-layer Nb_2P can most easily produce deformation under extrinsic loads than other M_2Ps. Electronic band structures were calculated with both using GGA-PBE and HSE06 functional as illustrated in **Figures S3** and **S4**. These four single-layer M_2Ps exhibit intrinsic electronic conductivity. Such soft 2D materials with metallic conductivity could pave the way for flexible conducting material and electronic devices, such as the 2H-Mo_2P as an anode material for Li- and Na-ion rechargeable batteries[30].

Table 2 Elastic properties of monolayer M_2P structures calculated by using GGA-PBE functional (elastic constants c_{ij}, layer modulus γ, shear modulus G^{2D}, in-plane stiffness S in N/m and dimensionless Poisson's ratio) and the effective single-layer thickness t in nm.

	t	c_{11}	c_{22}	c_{12}	$G^{2D}=c_{66}$	γ	$S_{[10]}$	$S_{[01]}$	$v^{2D}_{[10]}$	$v^{2D}_{[01]}$
Mo_2P	1.55	81.2	81.2	47.3	16.9	64.3	53.6	53.6	0.583	0.583

W_2P	1.68	83.0	83.0	53.7	14.7	68.3	48.3	48.3	0.647	0.647
Nb_2P	1.60	56.0	56.0	53.8	1.1	54.9	4.3	4.3	0.961	0.961
Ta_2P	1.52	88.7	88.7	47.7	20.5	68.2	63.0	63.0	0.538	0.538

3.3 Thermodynamic properties

The lattice thermal conductivity of single-layer M_2P was characterized by linearized Boltzmann transport equation within the single-mode RTA as following

$$\kappa = \frac{1}{NV_0}\sum_{\lambda} C_\lambda \mathbf{v}_\lambda \otimes \mathbf{v}_\lambda \tau_\lambda \tag{4}$$

where N is the total number of q points sampling the Brillouin zone, V_0 denotes the volume of a unit cell. λ is phonon mode, and C_λ, $\mathbf{v}_\lambda$, τ_λ, is the specific heat, phonon velocity, phonon lifetime. However, single-layer M_2P is 2D crystals in which vacuum thickness exists in the lattice. One thing must be considered that Eq. (4) is suitable for bulk structures. Hence, the thermal conductivity tensors need to be normalized by using V to substitute V_0. According to the effective single-layer thickness in **Table 2**, V is derived from V_0 subtracting vacuum volume. As shown in **Figure 4**, the lattice thermal conductivities (κ_{xx}=κ_{yy}) of single-layer M_2P decrease with the increasing temperature. Among of these four M_2P, the lattice thermal conductivity ranks as Mo_2P < W_2P < Nb_2P < Ta_2P throughout the temperature range (100–350 K). The calculated lattice thermal conductivities of monolayer Mo_2P, W_2P, Nb_2P, Ta_2P at room-temperature (300 K) are 3.54, 10.56, 12.81 and 51.11 $Wm^{-1}K^{-1}$. Thermal conductivity of Ta_2P is the highest among all M_2Ps and about 1344% larger than that of Mo_2P, as well as thermal conductivity of single-layer W_2P and Nb_2P are about 198% and 262% larger than that of Mo_2P monolayer, respectively. The lattice thermal conductivities of Ta_2P, W_2P and Nb_2P are

contradictory to the classical theory which suggests much heavier atom mass results in a smaller thermal conductivity[44].

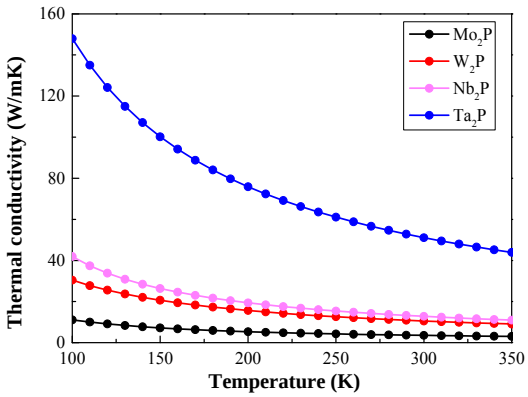

Figure 4 Lattice thermal conductivity $\kappa_{xx}=\kappa_{yy}$ of 2H-M_2P (M= Mo, W, Nb, Ta) at temperatures from 100 to 350 K with 10 K step are depicted filled circles and the values are fit by the color solid curves.

As depicted in **Figure S5,** most phonon lifetimes of acoustic branches of W_2P, Nb_2P and Ta_2P are larger than that of acoustic branches of Mo_2P, indicating strong phonon scattering in Mo_2P. Besides that, most phonon lifetimes of acoustic phonon modes are larger than those of optical branches. These results reflect the dominant contribution changes from the acoustic phonon modes to the total lattice thermal conductivity[45]. Weaker phonon-phonon scattering rate is observed in W_2P, Nb_2P and Ta_2P, which declares a much higher thermal conductivity. Moreover, the frequency dependent mode-Grüneisen parameters of M_2P in the irreducible Brillouin zone are calculated as illustrated in **Figure 5**. Mode-Grüneisen parameters (0 K) can provide anharmonicity information of phonon modes, determining the intrinsic phonon-phonon scattering. As shown in **Figure. 5(c)**, the Grüneisen parameters of acoustic phonon branches of single-layer Nb_2P is smaller than that of others, indicating weak anharmonic phonon scattering.

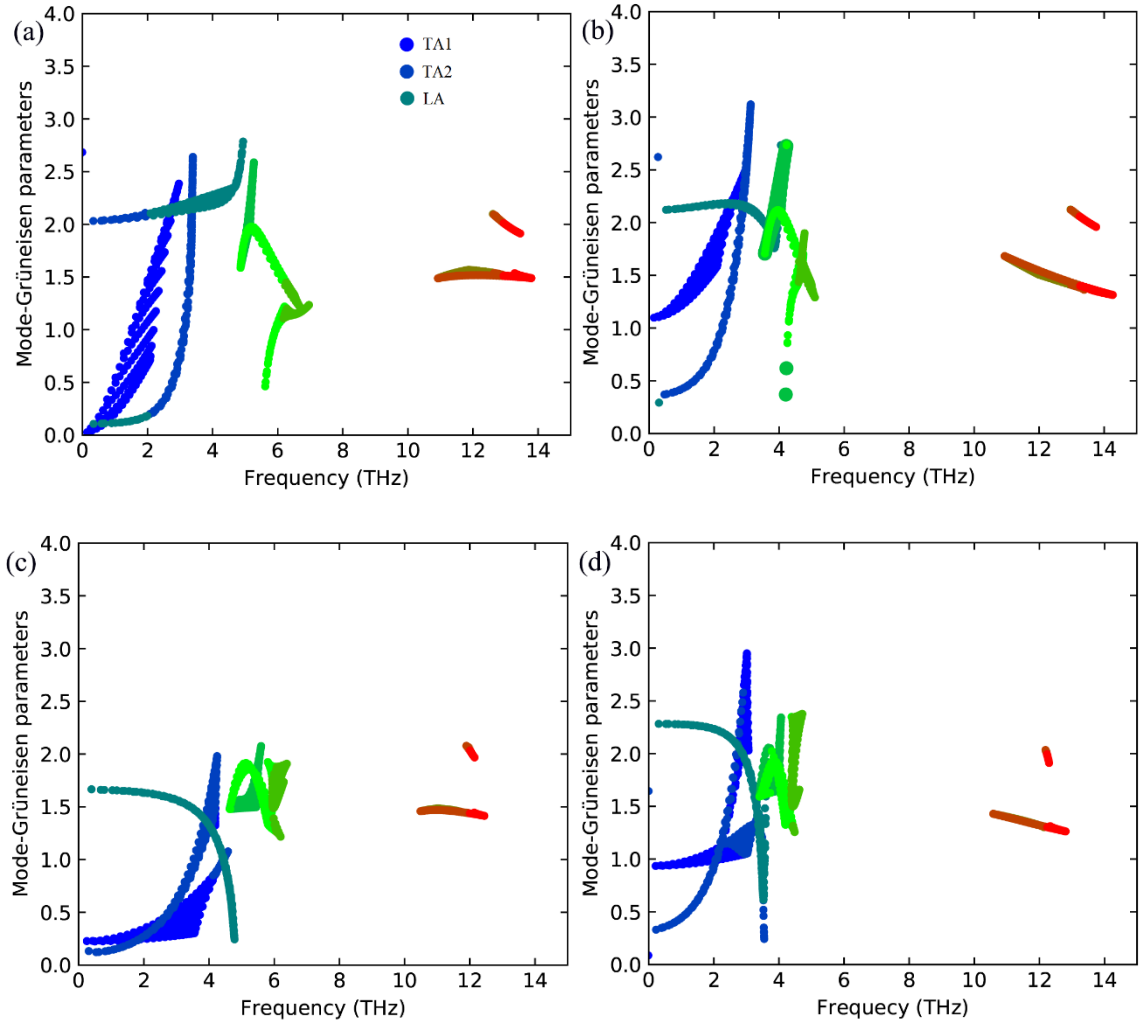

Figure 5 Mode-Grüneisen parameters of (a) Mo_2P, (b) W_2P, (c) Nb_2P and (d) Ta_2P. In (a) TA1, TA2 and LA are acoustic phonon branches, the points in other colors represent six optical branches, respectively.

Quasi-harmonic approximation (QHA) is performed to calculate thermal expansion and heat capacity at constant pressure (C_P). Phonon properties vary since the crystal potential is an anharmonic function of volume, but the harmonic approximation is simply applied to each volume[39]. Here, different volumes are introduced for these calculations by scaling equilibrium lattice constants a (b) between the scaling factors of -1.7%~3.2%. As illustrated in **Figure S6**, the phonon spectra under minimum strain (-1.7%) and maximum strain (3.2%) demonstrate that the strained structures are dynamical stability. Bulk modulus B, thermal expansion coefficients, average Grüneisen parameter γ and Helmholtz Free energy with respect to volume at different

temperature are calculated as illustrated in **Figure 6**. As the calculation of thermal conductivity, the vacuum thickness of M_2P crystals among ten volume points chosen are eliminated. Calculated Helmholtz free energy *F(T;V)* is described by the solid circle symbols in **Figure 6d**. Here, the equation of states (EOS) was adopted to fit the points [46]. The minimum values at different temperatures are depicted by the cross symbols. The calculated *B* of single-layer Mo_2P, W_2P, Nb_2P and Ta_2P is 69.84, 78.33, 58.69 69.43 GPa at 300 K, respectively. Among these four 2D crystals, *B* of Nb_2P decreases more rapidly with increasing temperature than other three structures. As shown in **Figure 6a**, however, monolayer Nb_2P exhibits the highest thermal expansion, which increases more quickly with increasing temperature. It can be attributed to its strongest anharmonic vibrations (**Figure 6c**)[47]. These results of Nb_2P further confirm its malleability which has been proved by the calculated lowest in-plane stiffness. As shown in **Figure 6b**, the present lowest thermal expansion of single-layer Ta_2P should be attributed to its weak anharmonicity (**Figure 6c**) which also results in a higher thermal conductivity.

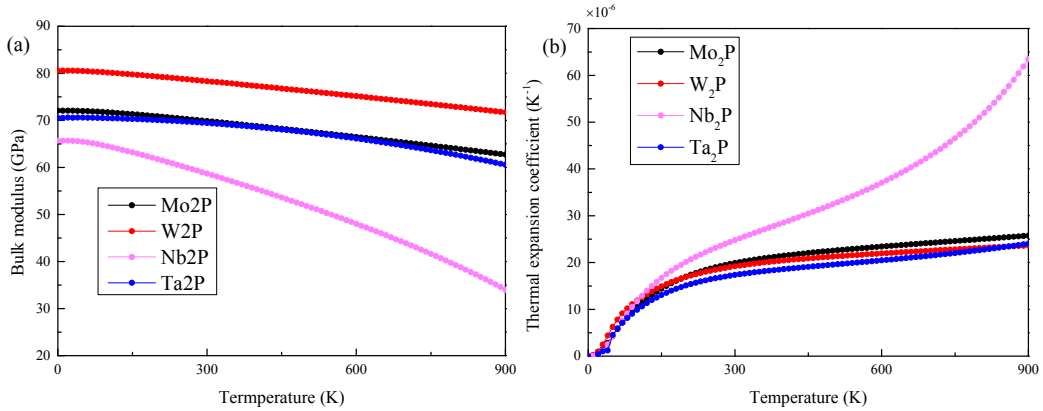

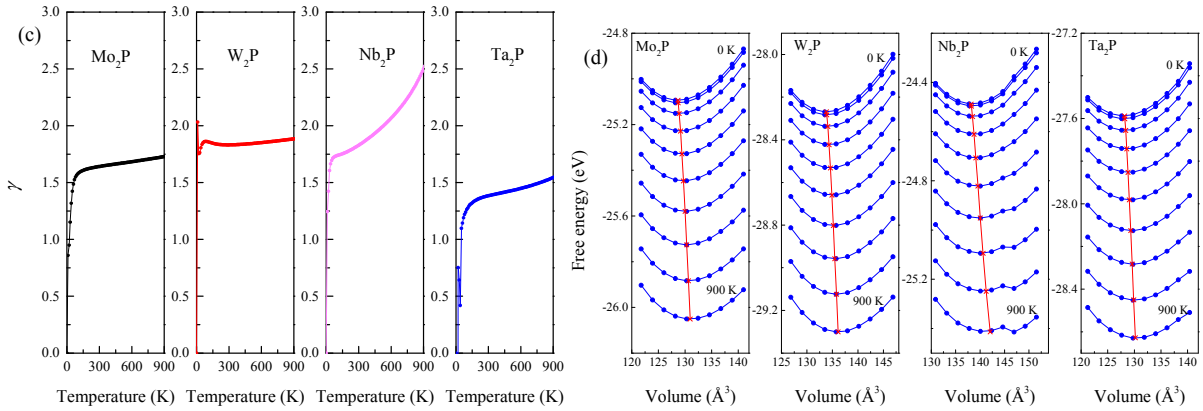

Figure 6 Temperature-dependent (a) bulk modulus, (b) volumetric thermal expansion coefficient and (c) average Grüneisen parameter of single-layer M_2P at finite temperature. (d) Helmholtz free energy of single-layer with respect to volume at temperatures from 0 to 900 K with 100 K steps is depicted by solid circles and the values are fit by the blue color solid curves. Cross symbols show the energy bottoms of the respective curves and simultaneously the equilibrium volumes. Lines connecting the cross symbols are guides to the view.

4. Conclusions

In summary, metallic 2D transition metal phosphides (Mo_2P, W_2P, Nb_2P and Ta_2P), confirmed by dynamical and thermal stabilities, are investigated by using first-principles calculations. Higher cohesive energy of M_2P than that of Mo_2S indicates the strong bonding structures in M_2Ps. The calculated electronic properties demonstrate these 2D crystals are metallic which are further confirmed by more accurate HSE06 functional. Calculated elastic properties proved that single-layer M_2P structures are softer materials due to their smaller stiffness than that of MoS_2, associating with excellently lateral deformation. Nb_2P is the softest material among M_2Ps because of its lowest stiffness and bulk modulus. These results are confirmed by the calculations of the highest thermal expansion and lowest bulk modulus. The calculated phonon lifetimes at room temperature (300 K) of M_2P demonstrate the dominant contribution changes from the acoustic phonon modes

to the total lattice thermal conductivity. Nb_2P shows the lowest bulk modulus and the highest thermal expansion because of its larger average Grüneisen parameter at finite temperature. The calculations also prove that the thermal conductivity of Ta_2P is the highest among the four materials, as well as the lowest thermal expansion, owing to its weak anharmonic phonon scattering. We believe that these four two dimensional 2H phase transition metal phosphides will be synthesized in the very near future. Our fundamental studies can guide the experimental and theoretical investigations in probing new 2D transition metal compounds.

Acknowledgements

The financial support from the National Natural Science Foundation of China (No. 51002128 and 51401176) and Scientific Research Foundation of Hunan Provincial Education Department (No.17A205) is greatly acknowledged.

References

[1] Novoselov K S, Geim A K, Morozov S V, Jiang D, Zhang Y, Dubonos S V, Grigorieva I V and Firsov A A 2004 Electric field effect in atomically thin carbon films *science* 306 666-669

[2] Lee C, Wei X, Kysar J W and Hone J 2008 Measurement of the elastic properties and intrinsic strength of monolayer graphene *science* 321 385-388

[3] Bolotin K I, Sikes K, Jiang Z, Klima M, Fudenberg G, Hone J, Kim P and Stormer H 2008 Ultrahigh electron mobility in suspended graphene *Solid State Communications* 146 351-355

[4] Balandin A A, Ghosh S, Bao W, Calizo I, Teweldebrhan D, Miao F and Lau C N 2008 Superior thermal conductivity of single-layer graphene *Nano letters* 8 902-907

[5] Yoo E, Kim J, Hosono E, Zhou H-S, Kudo T and Honma I 2008 Large reversible Li storage of graphene nanosheet families for use in rechargeable lithium ion batteries *Nano letters* 8 2277-2282

[6] Xia F, Farmer D B, Lin Y-M and Avouris P 2010 Graphene Field-Effect Transistors with High On/Off Current Ratio and Large Transport Band Gap at Room Temperature *Nano Letters* 10 715-718

[7] Luo K, Chen S and Duan C 2015 Indirect-direct band gap transition of two-dimensional arsenic layered semiconductors—cousins of black phosphorus *Science China Physics, Mechanics & Astronomy* 58 1-7

[8] Bozhao W, Xinghui L, Jiuren Y and Hyoyoung L 2017 Bulk β -Te to few layered β -tellurenes: indirect to direct band-Gap transitions showing semiconducting property *Materials Research Express* 4 095902

[9] Tang Q, Bao J, Li Y, Zhou Z and Chen Z 2014 Tuning band gaps of BN nanosheets and nanoribbons via interfacial dihalogen bonding and external electric field *Nanoscale* 6 8624-8634

[10] Liu L, Feng Y and Shen Z 2003 Structural and electronic properties of h-BN *Physical Review B* 68 104102

[11] Zhang J, Ren J, Fu H, Ding Z, Li H and Meng S 2015 Two-dimensional silicon-carbon hybrids with a honeycomb lattice: New family for two-dimensional photovoltaic materials *SCIENCE CHINA Physics, Mechanics & Astronomy* 58 106801

[12] Wu B, Yin J, Ding Y and Zhang P 2017 A new two-dimensional TeSe2 semiconductor: indirect to direct band-gap transitions *Science China Materials* 60 747-754

[13] Ma Y, Dai Y, Guo M, Niu C, Zhu Y and Huang B 2012 Evidence of the Existence of Magnetism in Pristine VX2 Monolayers (X = S, Se) and Their Strain-Induced Tunable Magnetic Properties *ACS Nano* 6 1695-1701

[14] Zhihao Y and Xinran W 2016 Transition-metal dichalcogenides: Group-10 expands the spectrum *SCIENCE CHINA Physics, Mechanics & Astronomy* 59 107031

[15] Naguib M, Kurtoglu M, Presser V, Lu J, Niu J, Heon M, Hultman L, Gogotsi Y and Barsoum M W 2011 Two‐dimensional nanocrystals produced by exfoliation of Ti3AlC2 *Advanced Materials* 23 4248-4253

[16] Naguib M, Mashtalir O, Carle J, Presser V, Lu J, Hultman L, Gogotsi Y and Barsoum M W 2012 Two-dimensional transition metal carbides *ACS nano* 6 1322-1331

[17] Naguib M and Gogotsi Y 2014 Synthesis of two-dimensional materials by selective extraction *Accounts of chemical research* 48 128-135

[18] Zhou J, Zha X, Zhou X, Chen F, Gao G, Wang S, Shen C, Chen T, Zhi C and Eklund P 2017 Synthesis and electrochemical properties of two-dimensional hafnium carbide *ACS nano* 11 3841-3850

[19] Zhou J, et al. 2017 Synthesis and Electrochemical Properties of Two-Dimensional Hafnium Carbide *ACS Nano*

[20] Coleman J N, Lotya M, O'neill A, Bergin S D, King P J, Khan U, Young K, Gaucher A, De S and Smith R J 2011 Two-dimensional nanosheets produced by liquid exfoliation of layered materials *Science* 331 568-571

[21] Khazaei M, Arai M, Sasaki T, Chung C Y, Venkataramanan N S, Estili M, Sakka Y and Kawazoe Y 2013 Novel electronic and magnetic properties of two‐dimensional transition metal carbides and nitrides *Advanced Functional Materials* 23 2185-2192

[22] Zha X-H, Zhou J, Zhou Y, Huang Q, He J, Francisco J S, Luo K and Du S 2016 Promising electron mobility and high thermal conductivity in Sc 2 CT 2 (T= F, OH) MXenes *Nanoscale* 8 6110-6117

[23] Zha X-H, Huang Q, He J, He H, Zhai J, Francisco J S and Du S 2016 The thermal and electrical properties of the promising semiconductor MXene Hf2CO2 *Scientific reports* 6 27971

[24] Byeon A, Zhao M-Q, Ren C E, Halim J, Kota S, Urbankowski P, Anasori B, Barsoum M W and Gogotsi Y 2017 Two-Dimensional Titanium Carbide MXene As a Cathode Material for Hybrid Magnesium/Lithium-Ion Batteries *ACS Applied Materials & Interfaces* 9 4296-4300

[25] Sun Q, Dai Y, Ma Y, Jing T, Wei W and Huang B 2016 Ab initio prediction and characterization of Mo2C monolayer as anodes for lithium-ion and sodium-ion batteries *The journal of physical chemistry letters* 7 937-943

[26] Gogotsi Y 2015 Chemical vapour deposition: transition metal carbides go 2D *Nature materials* 14 1079

[27] Xu C, Wang L, Liu Z, Chen L, Guo J, Kang N, Ma X-L, Cheng H-M and Ren W 2015 Large-area high-quality 2D ultrathin Mo2C superconducting crystals *Nature materials* 14 1135

[28] Geng D, Zhao X, Chen Z, Sun W, Fu W, Chen J, Liu W, Zhou W and Loh K P 2017 Direct Synthesis of Large‐Area 2D Mo2C on In Situ Grown Graphene *Advanced Materials*

[29] Lei J, Kutana A and Yakobson B I 2017 Predicting stable phase monolayer Mo 2 C (MXene), a superconductor with chemically-tunable critical temperature *Journal of Materials Chemistry C*

[30] Mortazavi B, Shahrokhi M, Makaremi M and Rabczuk T 2017 Theoretical realization of Mo 2 P; a novel stable 2D material with superionic conductivity and attractive optical properties *Applied Materials Today* 9 292-299

[31] Kresse G and Hafner J 1994 Norm-conserving and ultrasoft pseudopotentials for first-row and transition elements *Journal of Physics: Condensed Matter* 6 8245

[32] Kresse G and Furthmüller J 1996 Efficiency of ab-initio total energy calculations for metals and semiconductors using a plane-wave basis set *Computational materials science* 6 15-50

[33] Kresse G and Furthmüller J 1996 Efficient iterative schemes for ab initio total-energy calculations using a plane-wave basis set *Physical review B* 54 11169

[34] Blöchl P E 1994 Projector augmented-wave method *Physical review B* 50 17953

[35] Perdew J P, Burke K and Ernzerhof M 1996 Generalized gradient approximation made simple *Physical review letters* 77 3865

[36] Wang Y, Wang S-S, Lu Y, Jiang J and Yang S A 2016 Strain-induced isostructural and magnetic phase transitions in monolayer MoN2 *Nano letters* 16 4576-4582

[37] Heyd J, Scuseria G E and Ernzerhof M 2003 Hybrid functionals based on a screened Coulomb potential *The Journal of Chemical Physics* 118 8207-8215

[38] Baroni S, De Gironcoli S, Dal Corso A and Giannozzi P 2001 Phonons and related crystal properties from density-functional perturbation theory *Reviews of Modern Physics* 73 515

[39] Togo A and Tanaka I 2015 First principles phonon calculations in materials science *Scripta Materialia* 108 1-5

[40] Togo A, Chaput L and Tanaka I 2015 Distributions of phonon lifetimes in Brillouin zones *Physical Review B* 91 094306

[41] Becke A D and Edgecombe K E 1990 A simple measure of electron localization in atomic and molecular systems *The Journal of chemical physics* 92 5397-5403

[42] Andrew R C, Mapasha R E, Ukpong A M and Chetty N 2012 Mechanical properties of graphene and boronitrene *Physical Review B* 85 125428

[43] Grimme S, Antony J, Ehrlich S and Krieg H 2010 A consistent and accurate ab initio parametrization of density functional dispersion correction (DFT-D) for the 94 elements H-Pu *The Journal of chemical physics* 132 154104

[44] Srivastava G P. The physics of phonons. Place Published: CRC press,1990:

[45] Guo S-D 2017 Anisotropic lattice thermal conductivity in three-fold degeneracy topological semimetal MoP: a first-principles study *Journal of Physics: Condensed Matter* 29 435704

[46] Vinet P, Rose J H, Ferrante J and Smith J R 1989 Universal features of the equation of state of solids *Journal of Physics: Condensed Matter* 1 1941

[47] Peng B, Zhang H, Shao H, Xu Y, Zhang X and Zhu H 2016 Thermal conductivity of monolayer MoS 2, MoSe 2, and WS 2: interplay of mass effect, interatomic bonding and anharmonicity *RSC Advances* 6 5767-5773